Human Molecular Genetics, 2017, Vol. 26, No. 19 3736–3748

doi: 10.1093/hmg/ddx258
Advance Access Publication Date: 6 July 2017
Original Article

ORIGINAL ARTICLE

Expression of the neuropathy-associated *MTMR2* gene rescues *MTM1*-associated myopathy

Matthieu A. Raess[1,2,3,4,5], Belinda S. Cowling[1,2,3,4], Dimitri L. Bertazzi[5], Christine Kretz[1,2,3,4], Bruno Rinaldi[5], Jean-Marie Xuereb[6], Pascal Kessler[1,2,3,4], Norma B. Romero[8,9,10], Bernard Payrastre[6,7], Sylvie Friant[5,†] and Jocelyn Laporte[1,2,3,4,*,†]

[1]Institut de Génétique et de Biologie Moléculaire et Cellulaire (IGBMC), 67404 Illkirch, France, [2]INSERM U964, 67404 Illkirch, France, [3]CNRS, UMR7104, 67404 Illkirch, France, [4]Université de Strasbourg, 67404 Illkirch, France, [5]Department of Molecular and Cellular Genetics, Université de Strasbourg, CNRS, GMGM UMR7156, 67000 Strasbourg, France, [6]INSERM U1048 and Université Toulouse 3, Institut des Maladies Métaboliques et Cardiovasculaires (I2MC), 31432 Toulouse, France, [7]CHU de Toulouse, Laboratoire d'Hématologie, 31059 Toulouse, France, [8]INSERM UMRS974, CNRS FRE3617, Center for Research in Myology, Pitié-Salpêtrière Hospital, Sorbonne Universities, Pierre and Marie Curie University, 75013 Paris, France, [9]Unit of Neuromuscular Morphology, Institute of Myology and [10]Reference Center for Neuromuscular Pathology Paris-East, Institute of Myology, Public Hospital Network of Paris, Pitié-Salpêtrière Hospital, 75013 Paris, France

*To whom correspondence should be addressed at: Department of Translational Medicine, IGBMC, 1 rue Laurent Fries, BP10142, 67404 Illkirch, France. Tel: +33 388653412; Fax: +33 388653201; Email: jocelyn@igbmc.fr

Abstract

Myotubularins (MTMs) are active or dead phosphoinositides phosphatases defining a large protein family conserved through evolution and implicated in different neuromuscular diseases. Loss-of-function mutations in MTM1 cause the severe congenital myopathy called myotubular myopathy (or X-linked centronuclear myopathy) while mutations in the MTM1-related protein MTMR2 cause a recessive Charcot-Marie-Tooth peripheral neuropathy. Here we aimed to determine the functional specificity and redundancy of MTM1 and MTMR2, and to assess their abilities to compensate for a potential therapeutic strategy. Using molecular investigations and heterologous expression of human MTMs in yeast cells and in *Mtm1* knockout mice, we characterized several naturally occurring MTMR2 isoforms with different activities. We identified the N-terminal domain as responsible for functional differences between MTM1 and MTMR2. An N-terminal extension observed in MTMR2 is absent in MTM1, and only the short MTMR2 isoform lacking this N-terminal extension behaved similarly to MTM1 in yeast and mice. Moreover, adeno-associated virus-mediated exogenous expression of several MTMR2 isoforms ameliorates the myopathic phenotype owing to MTM1 loss, with increased muscle force, reduced myofiber atrophy, and reduction of the intracellular disorganization hallmarks associated with myotubular myopathy. Noteworthy, the short MTMR2 isoform provided a better rescue when compared with the long MTMR2 isoform. In conclusion, these results point to the molecular basis for MTMs functional specificity. They also provide the proof-of-concept that expression of the neuropathy-associated *MTMR2* gene improves the *MTM1*-associated myopathy, thus identifying *MTMR2* as a novel therapeutic target for myotubular myopathy.

[†]These authors contributed equally to this work.

Received: March 5, 2017. **Revised:** June 27, 2017. **Accepted:** June 28, 2017

Introduction

Myotubularin (MTM1) and MTM-related proteins (MTMR) define a conserved protein family implicated in different neuromuscular diseases (1). They have been classified in the phosphatase super-family. In humans, eight MTMs share the C(X)5R motif found in tyrosine and dual-specificity phosphatases and display enzymatic activity, while the six others lack this motif and are nicknamed dead-phosphatases. Unexpectedly, it was found that enzymatically active MTMs do not act on proteins but dephosphorylate phosphoinositides (PPIn), lipids concentrated in specific membrane sub-domains (2,3). PPIn are lipid second messengers implicated in a wide range of cellular processes including signaling and intracellular organization (4). MTMs are PPIn 3-phosphatases that dephosphorylate the phosphatidylinositol (PtdIns) 3-phosphate (PtdIns3*P*) and the PtdIns 3,5-bisphosphate (PtdIns(3,5)P_2), leading to the production of PtdIns5*P* (2,3,5–7). PtdIns5*P* is implicated in transcriptional regulation and growth factor signaling, while PtdIns3*P* and PtdIns(3,5)P_2 regulate membrane trafficking and autophagy. PtdIns3*P* is produced through the phosphorylation of PtdIns by class II and III PtdIns 3-kinases and PtdIns(3,5)P_2 is obtained mainly from the phosphorylation of PtdIns3*P* by PIKfyve (8,9). They recruit proteins to specific endosomal pools or to particular endoplasmic reticulum sites where autophagosomes are formed. For example, the Fab1-YOTB-Vac1-EEA1 (FYVE) domain of EEA1 binds specifically PtdIns3*P* concentrated on early endosomes to regulate endosomal fusion and cargo delivery (9). Dead MTMs oligomerize with and regulate the enzymatic activity and/or subcellular localization of their active homologs (10–12). In addition to the active or dead phosphatase domain, MTMs share a Pleckstrin Homology, Glucosyltransferase, Rab-like GTPase Activator and MTM (PH-GRAM) domain that bind to PPIn or proteins, and a coiled-coil domain implicated in their oligomerization (1).

There are 14 MTMs in human and one active MTM in yeast *Saccharomyces cerevisiae* (1,13). The yeast MTM Ymr1 regulates vacuole protein sorting and its absence induces vacuolar fragmentation (14). Expression of human MTM1 in yeast leads to the enlargement of the vacuole as a consequence of its phosphatase activity and PtdIns3*P* decrease (2,15). In human, mutations in *MTM1* cause the severe congenital myopathy called myotubular myopathy [or X-linked centronuclear myopathy (XLCNM); OMIM 310400] (16), while mutations in either the active *MTMR2* or the dead-phosphatase *MTMR13* cause Charcot-Marie-Tooth (CMT) peripheral neuropathies (CMT4B1, OMIM 601382 and CMT4B2, OMIM 604563, respectively) (17–19). In addition, putative mutations in *MTMR5* (Sbf1) were linked to CMT4B3 (OMIM 615284) and axonal neuropathy (20–22). Thus, lack of one MTM is not fully compensated by its homologs, despite the fact they are ubiquitously expressed. Moreover, the related diseases affect different tissues. Of note, MTM1 and MTMR2 are part of the same evolutionary sub-group based on their sequence (13). Thus, this suggests uncharacterized tissue-specific functions potentially reflecting different protein isoforms having specific activities or interactors. Here, we show that there are two protein isoforms of MTMR2 and we studied their *in vivo* functions in yeast and in mice. We report that only the short MTMR2 isoform complements the yeast *ymr1*Δ mutant phenotypes at a similar level as MTM1. Moreover, both MTMR2 isoforms ameliorate the myopathy phenotypes displayed by *Mtm1* knockout (KO) mice, and specifically the short MTMR2 isoform produced a better disease rescue.

Results

MTMR2 splicing variants are differentially expressed and encode for long and short protein isoforms

Mutations in the *MTMR2* gene are responsible for CMT neuropathy (CMT4B1) whereas mutations in *MTM1* lead to X-linked centronuclear myopathy (XLCNM), suggesting that these two ubiquitously expressed MTMs have distinct functions. Most tissues contain more than a single isoform, thus their localization and extent of expression could help explain their different functions. In order to investigate MTMR2 function, we first defined its tissue expression and isoforms. In mice, four *MTMR2* mRNA isoforms (V1 to V4) have been previously reported in peripheral nerves, potentially coding for 2 protein isoforms (Supplementary Material, Fig. S1A and B) (23). Variants V2 to V4 differ from variant V1 by the inclusion of alternative exons 1a and/or 2a leading to a premature stop codon and unmasking an alternative start site in exon 3. Variant V1 encodes a 643 amino acids (Aa) protein that we named MTMR2-L (long) while the other isoforms code for a 571 Aa protein named MTMR2-S (short) that was previously detected in various cell lines (23). The two protein isoforms differ only in their translation start sites; MTMR2-S starts right before the PH-GRAM domain while the MTMR2-L has an extended N-terminal sequence without known homology to any protein domain and that was not visible in the crystal structure (Fig. 1C; Supplementary Material, Fig. S1B) (24,25). The expression level of these isoforms was first investigated in human tissues through mining the GTEx expression database encompassing data on 51 human tissues (26). Variant V1 is the major *MTMR2* RNA in brain, liver and spleen while variant V2 is predominant in the other tissues. The different variants were only poorly expressed in skeletal muscle (Fig. 1A). In mouse, RT-PCR and Sanger sequencing confirmed the existence of the four *Mtmr2* mRNA variants (V1 to V4) in tibialis anterior (TA) skeletal muscle of wild-type (WT) and *Mtm1* KO mice and in the liver (Supplementary Material, Fig. S1C and D), suggesting that both MTMR2-L and MTMR2-S proteins are present in skeletal muscle.

Short but not long MTMR2 isoform displays an MTM1-like activity in yeast cells

To compare the cellular function of MTM1, MTMR2-L and MTMR2-S proteins *in vivo*, we used heterologous expression of these human MTMs in yeast cells. Yeast is a good model to study phosphoinositide-dependent membrane trafficking as it is conserved from yeast to higher eukaryotes (27). In yeast cells, vacuole volume, morphology, acidity and membrane potential are controlled by PtdIns(3,5)P_2 that is produced through the phosphorylation of PtdIns3*P* by Fab1/PIKfyve kinase. In *fab1*Δ mutant cells, the vacuole is very large and unilobed owing to low levels of PtdIns(3,5)P_2 (15,28,29). On the contrary, *ymr1*Δ cells lacking the unique yeast MTM have fragmented vacuoles owing to excess of PtdIns(3,5)P_2 and/or PtdIns3*P* (14), and this phenotype is complemented by the expression of the human MTM1 that induces a large vacuole phenotype (15). To determine MTM1, MTMR2-L and MTMR2-S intracellular localization, we overexpressed GFP-tagged fusions in *ymr1*Δ cells. MTM1-GFP and MTMR2-S-GFP proteins were concentrated to a membrane punctate structure adjacent to the vacuole (also positive for the FM4-64 lipid dye), while MTMR2-L-GFP was mainly in the cytoplasm (Fig. 2C). We next assessed the vacuolar morphology upon overexpression of either GFP-tagged or untagged human

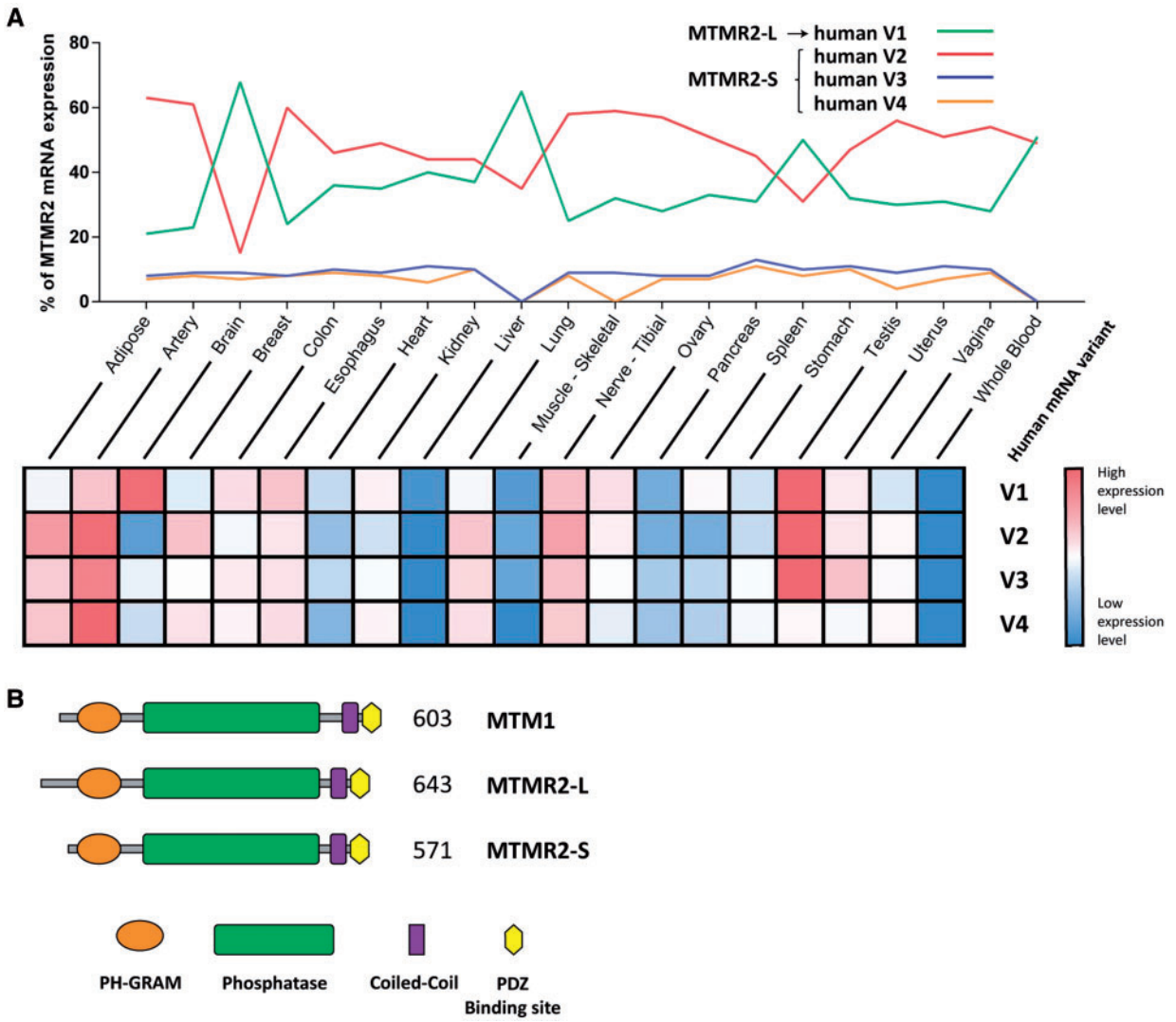

Figure 1. *MTMR2* splicing isoforms are differentially expressed and encode for long and short protein isoforms. (**A**) Comparative expression of *MTMR2* mRNA isoforms V1 to V4 in 20 human tissues from GTEx database mining (top). Human *MTMR2* V2 isoform contains additional exons 1a and 2a compared with V1, V3 contains exon 1a and V4 contains exons 1a and 2b. Tissue expression of each isoform independently (bottom). (**B**) Protein domains of MTMR2-L encoded by V1 mRNA isoform, and MTMR2-S encoded by the other isoforms, compared to MTM1.

MTMs in *ymr1*Δ cells by staining the vacuolar membrane with the lipophilic dye FM4-64 (Fig. 2B and C). To detect MTMR2 isoforms, a mouse monoclonal antibody was raised against recombinant full length human MTMR2-L. This antibody was validated on the transformed yeast protein extracts, and specifically recognized MTMR2-L and MTMR2-S (Fig. 2A). Vacuoles were significantly enlarged upon expression of MTM1 or MTMR2-S in *ymr1*Δ cells while they remained fragmented with MTMR2-L. MTM1 and MTMR2-S induced a large vacuolar morphology mimicking a *fab1*Δ phenotype owing to the high expression levels of these phosphatases (overexpression plasmid). These results show that only the membrane localized MTM constructs rescued the vacuole morphology defects of *ymr1*Δ cells. Since the vacuolar morphology reflects the PtdIns(3,5)P_2 level and as PtdIns(3,5)P_2 is not abundant enough to be detected in normal growth conditions (29), we quantified by mass assay the level of PtdIns5P, the lipid produced by MTM phosphatase activity from PtdIns(3,5)P_2 (Fig. 2F). PtdIns5P level was increased by MTM1 and MTMR2-S overexpression in *ymr1*Δ cells, while MTMR2-L had no effect. We also quantified the PtdIns3P MTM substrate level, by counting the punctate structures that were positive for DsRED-FYVE, a reporter for PtdIns3P-enriched membranes (27) (Fig. 2D and E). Overexpression of MTM1 and MTMR2-S significantly reduced PtdIns3P level while MTMR2-L had no effect. However, previous data showed MTMR2-L had a strong phosphatase activity *in vitro* (5,7), suggesting that the cytoplasmic localization of this isoform in yeast cells does not allow PPIn substrate dephosphorylation. In conclusion, only MTMR2-S has a similar phosphatase activity and localization as MTM1 in yeast cells, while MTMR2-L behaves differently.

Exogenous expression of MTMR2 short isoform in the *Mtm1* KO mice rescues muscle weight and force similarly to MTM1 expression

To assess whether in mammals MTMR2-S is also functionally closer to MTM1 compared with MTMR2-L, we overexpressed human MTM1, MTMR2-L and MTMR2-S in the *Mtm1* KO mouse and analyzed different myopathy-like phenotypes. The

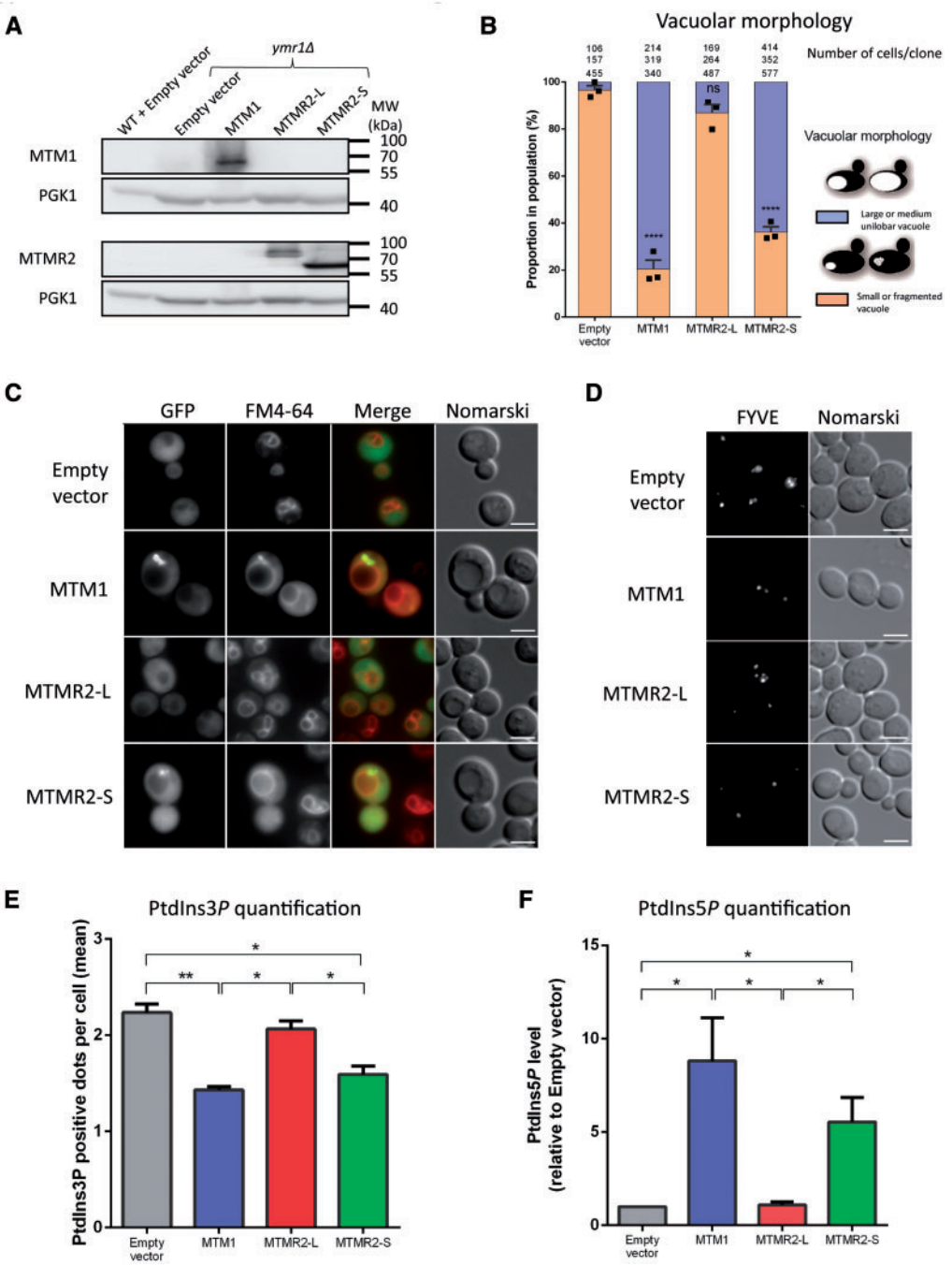

Figure 2. Short but not long MTMR2 isoform displays an MTM1-like activity. Exogenous expression of human MTM1 and MTMR2 long and short isoforms using the high copy number plasmid 2μ in *ymr1Δ* yeast cells. **(A)** Detection of exogenously expressed human myotubularins by western blot using anti-MTM1 or anti-MTMR2 antibodies, in two independents blots with the same samples. Wild-type (WT) and *ymr1Δ* yeast strains with empty vectors are used as controls. Pgk1p is used as a loading control. This blot is representative of at least three independent experiments. **(B)** Quantification of vacuolar morphology in yeast cells over-expressing untagged myotubularins. Three clones analyzed per constructs; the number of cells counted per clone is indicated above. Data represent mean ± S.E.M. ****$P < 0.0001$, ns, not significant (ANOVA test). **(C)** Localization of GFP-tagged human myotubularins. Vacuole morphology is assessed by the lipophilic dye FM4-64 and Nomarski differential contrast. *ymr1Δ* yeast cells and MTMR2-L expressing cells display a fragmented vacuole while MTM1 and MTMR2-S over-expressing cells have a large vacuole. Scale bar 5 μm. **(D)** FYVE punctuated localization in yeast clones expressing untagged myotubularins and DsRED-tagged FYVE domain that specifically binds PtdIns3P. Scale bar 5 μm. **(E)** PtdIns3P quantification by counting the number of FYVE-positive dots per cell, as represented in (D). PtdIns3P is decreased upon MTM1 and MTMR2-S expression but not with MTMR2-L. Data represent mean ± S.E.M. *$P < 0.05$, **$P < 0.01$ (ANOVA test). **(F)** PtdIns5P quantification by mass assay on total lipid extract from yeast cells over-expressing untagged myotubularins. Three clones analyzed per constructs. Data represent mean ± S.E.M. *$P < 0.05$ (ANOVA test).

different MTMs were expressed from adeno-associated virus (AAV) AAV2/1 under the control of the CMV promoter and the recombinant virions were injected into the TA muscles of 2- to 3-week-old *Mtm1* KO mice. The *Mtm1* KO mice develop a progressive muscle atrophy and weakness starting at 2–3 weeks and leading to death by 8 weeks, the TA muscle being the most affected muscle detected in this model (30,31). We have previously shown that AAV-mediated expression of MTM1 for

4 weeks in the TA muscle, corrects the myopathy phenotype in *Mtm1* KO mice (15). Therefore to determine the impact of introducing MTMR2-L and MTMR2-S into *Mtm1* KO mice, we followed our previously described protocol for AAV injections (15), using MTM1 as a positive control for the rescue, and empty AAV2/1 as a disease control in the contralateral muscle. The MTM1, MTMR2-L and MTMR2-S human MTMs were expressed in injected TA, as revealed from anti-MTM1 and anti-MTMR2 western blot analyses (Fig. 3A). Endogenous MTMR2 proteins were not detected in muscle injected with empty AAV, most likely owing to the low level of endogenous expression (Fig. 3A).

Four weeks after AAV injection, the TA muscle weight of the *Mtm1* KO mice was decreased by 2.5-fold compared with WT mice, both injected with empty AAV control. MTM1 or MTMR2-S expression in *Mtm1* KO mice increased muscle mass significantly compared with the empty AAV control (1.5-fold), contrary to MTMR2-L (Fig. 3B). To address a potential hypertrophic effect of human MTM1 or MTMR2 constructs in WT mice, TA muscle weight of injected WT mice was quantified (Supplementary Material, Fig. S2). No increased muscle mass was noted with any MTMs indicating that the amelioration observed in the *Mtm1* KO mice was not owing to a hypertrophic effect but to a functional rescue.

The *Mtm1* KO mice displayed very weak muscle force compared with WT mice, and all MTM constructs including MTMR2-L improved the TA specific muscle force (Fig. 3C). Noteworthy, a similar rescue was observed for MTM1 and MTMR2-S, significantly above that observed for MTMR2-L injected muscles. These results show that both MTMR2-L and MTMR2-S isoforms improve the muscle weakness owing to loss of MTM1, and MTMR2-S expression induces a rescue akin to that observed by MTM1 gene replacement.

The MTMR2 isoforms rescue the histopathological hallmarks of the *Mtm1* KO mouse

In the *Mtm1 KO* mice, TA injections of AAV2/1 carrying MTM1, MTMR2-L or MTMR2-S increased muscle mass (except for MTMR2-L) and force (Fig. 3). To analyze the rescue at the histological level, fiber size and nuclei localization were determined (Fig. 4). Hematoxylin-eosin (HE) staining revealed increased fiber size in AAV-MTM1 and AAV-MTMR2-S injected *Mtm1* KO muscles, compared to muscles treated with empty AAV or MTMR2-L (Fig. 4A), even though we observed spatial heterogeneity in the muscle, with some regions still displaying smaller atrophic fibers. Morphometric analysis revealed that among the different MTMs tested, MTM1 induced a clear shift toward larger fiber diameters compared with MTMR2 constructs and empty AAV (Fig. 4C). A very significant difference ($P < 0.0001$) was observed between AAV-MTM1 (mean 58.4%) and AAV-MTMR2-L (mean 26.2%) in the percentage of muscle fibers having an area above 800 μm^2, whereas the difference was less significant ($P = 0.033$) between MTM1 and MTMR2-S (39.8%) (Fig. 4D). Since nuclei are abnormally located within muscle fibers in *Mtm1* KO mice, we analyzed the distribution of nuclei. Injection of MTM1, MTMR2-S or MTMR2-L into the TA muscle of *Mtm1* KO increased significantly the percentage of well-positioned peripheral nuclei compared with contralateral control muscles injected with empty AAV (Fig. 4E). The succinate dehydrogenase (SDH) staining showed accumulation at the periphery and center in the *Mtm1* KO fibers (15), while it was greatly ameliorated upon expression of the different MTM constructs (Fig. 4B). These results show that both MTMR2 isoforms were able to ameliorate the

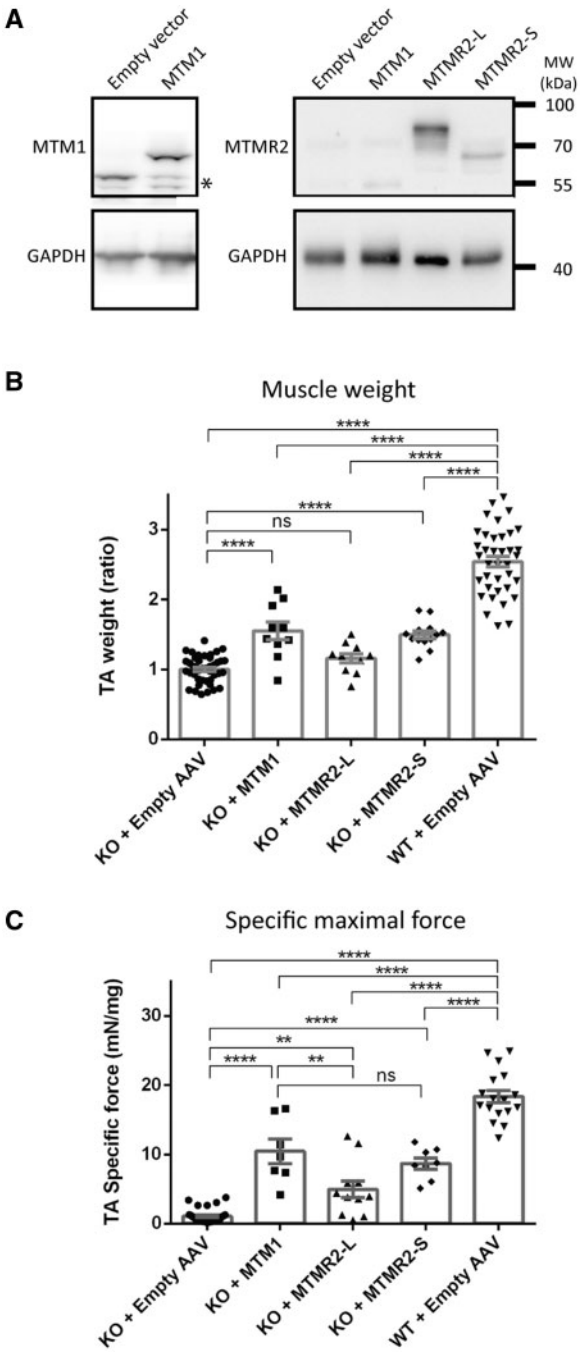

Figure 3. The MTMR2 short isoform rescues muscle weight and force similarly as MTM1 in *Mtm1* KO myopathic mice. TA muscles from 2- to 3-week-old *Mtm1* KO mice were injected with AAV2/1 expressing myotubularins and analyzed 4 weeks later. (**A**) Detection of exogenously expressed human myotubularins by western blot using anti-MTM1 or anti-MTMR2 antibodies; GAPDH is used as a loading control. Unspecific bands are indicated by a star. This blot is representative for each construct, and at least 10 muscles per construct were analyzed. (**B**) Ratio of muscle weight of TA expressing human myotubularins compared with the contralateral leg injected with empty AAV. MTMR2-S improved muscle mass similarly as MTM1 while MTMR2-L had no effect. A value of 1 was set for the *Mtm1* KO mice injected with empty AAV. $n > 10$. Data represents mean ± S.E.M. ****$P < 0.0001$, ns, not significant (ANOVA test). (**C**) Specific maximal force of TA muscle (absolute maximal force (mN) relative to muscle mass (mg)). Both MTMR2 isoforms improved muscle force. $n > 7$. Data represent means ± S.E.M. **$P < 0.01$, ****$P < 0.0001$; ns, not significant (ANOVA test).

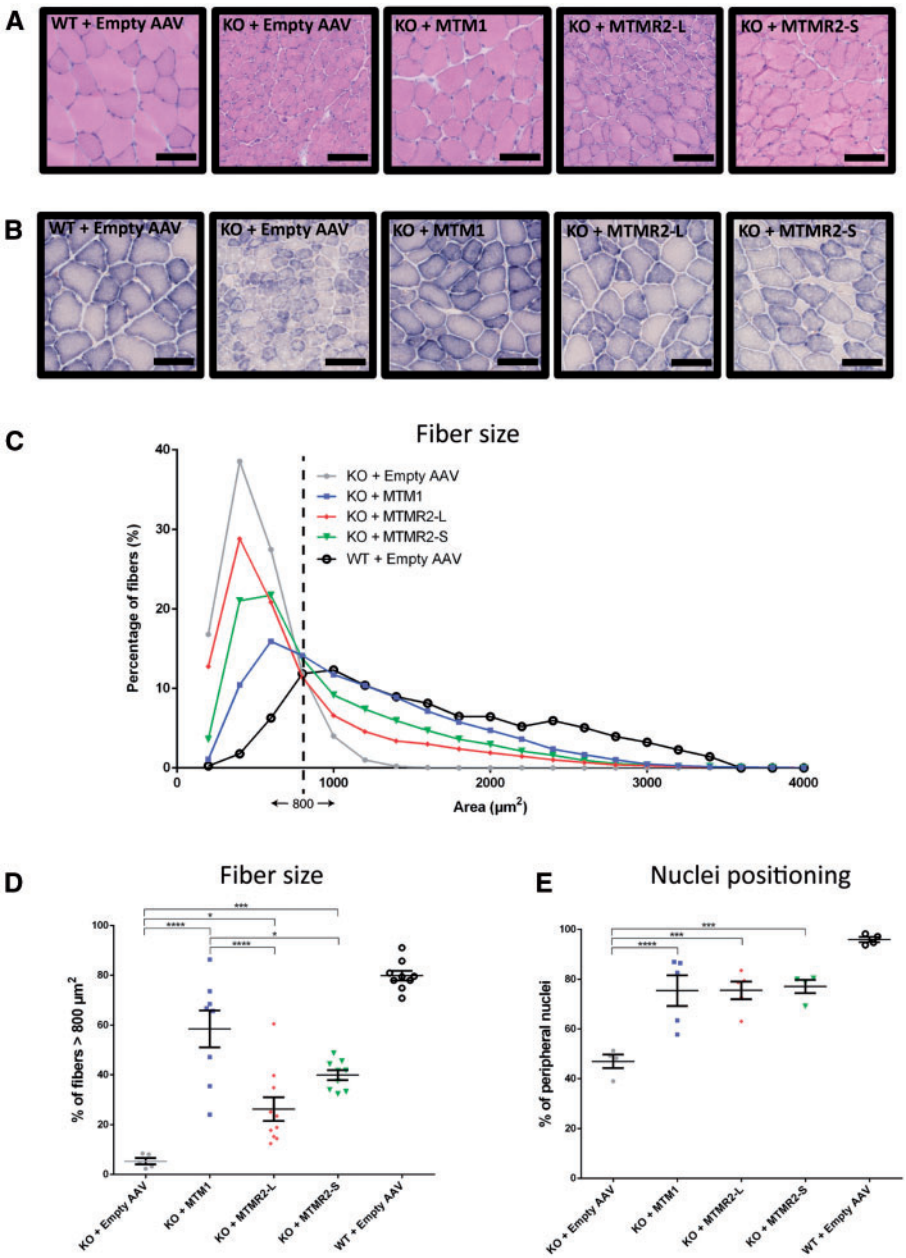

Figure 4. Both long and short MTMR2 isoforms improve the histological hallmarks of the *Mtm1* KO mouse. TA muscles from 2- to 3-week-old *Mtm1* KO mice were injected with AAV2/1 expressing myotubularins and analyzed 4 weeks later. **(A)** Hematoxylin-eosin staining of TA muscle sections. Scale bar 100 µm. **(B)** Succinate dehydrogenase (SDH) staining of TA muscle sections. Scale bar 100 µm. **(C)** Quantification of fiber area. Fiber size is grouped into 200 μm^2 intervals and represented as a percentage of total fibers in each group. $n > 1000$ for 8 mice. **(D)** Percentage of fibers above 800 μm^2. $n > 8$. Data represent mean ± S.E.M. $^*P < 0.05$, $^{***}P < 0.001$, $^{****}P < 0.0001$ (ANOVA test). The value for WT is statistically different from all *Mtm1* KO injected groups. **(E)** Nuclei positioning in TA muscle. Percentage of well-positioned peripheral nuclei. $n > 6$ animals. Data represent mean ± S.E.M. $^{***}P < 0.001$, $^{****}P < 0.0001$ (ANOVA test). The value for WT is statistically different from all *Mtm1* KO injected groups.

histopathological hallmarks of the MTM1 myopathy, where MTMR2-S was more effective.

MTMR2 isoforms rescue *Mtm1* KO muscle disorganization and normalize PtdIns3P levels

Patients with myotubular myopathy and the *Mtm1* KO mice display an intracellular disorganization of their muscle fibers at the ultrastructural level (30,32). To determine the organization of the contractile apparatus and triads, the ultrastructure of the different injected TA muscles was assessed by electron microscopy. As previously published, we observed Z-line and mitochondria misalignment, thinner sarcomeres and lack of well-organized triads in the *Mtm1* KO muscle injected with empty AAV (15) (Fig. 5A). Expression of MTM1 and both MTMR2 isoforms improved these different phenotypes, with the observation of well-organized triads with two sarcoplasmic reticulum cisternae associated with a central transverse-tubule (T-tubule) in muscles injected with MTM1, MTMR2-L or MTMR2-S (Fig. 5A). Moreover, AAV-mediated expression of MTM1, MTMR2-L and MTMR2-S increased the number of triads per sarcomere back to almost WT levels, with a better effect for MTMR2-S compared with MTMR2-L (Fig. 5B).

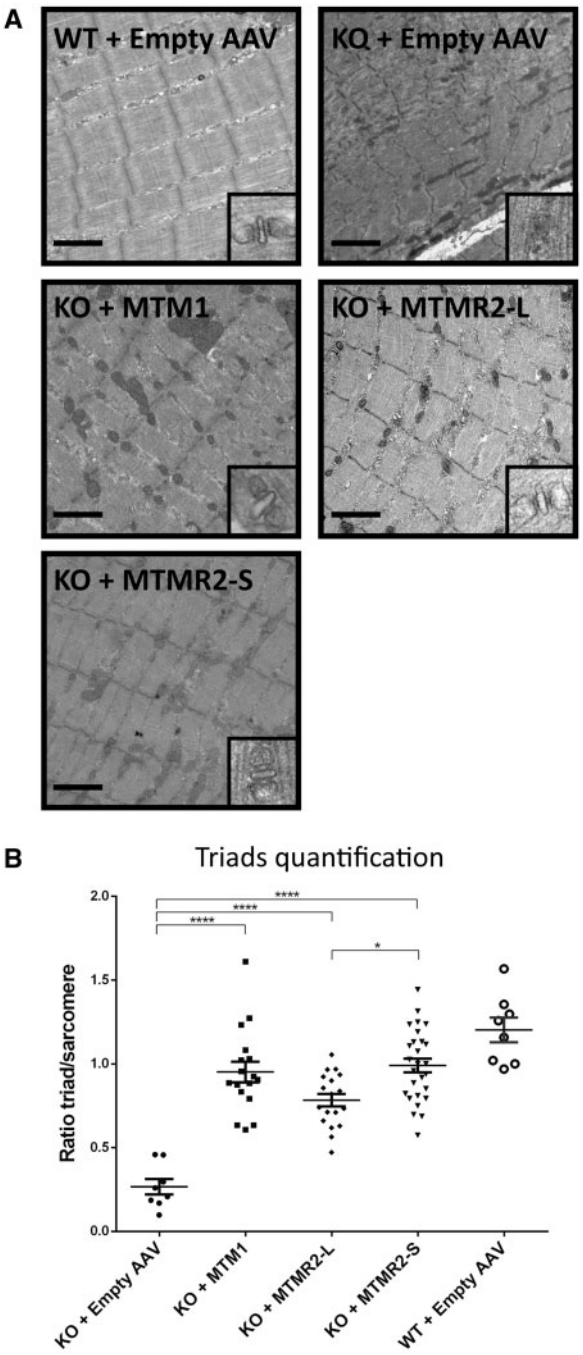

Figure 5. MTMR2 isoforms rescue the muscle ultrastructure and triad morphology of the *Mtm1* KO muscles. TA muscles from *Mtm1* KO mice were injected with AAV2/1 expressing myotubularins. (**A**) Electron microscopy pictures displaying sarcomere, mitochondria and triad organization. Scale bar 1 μm. Representative triads are displayed in the zoom square. (**B**) Quantification of the number of well-organized triads per sarcomere. $n > 20$ images for 2 mice each. All muscles expressing myotubularins were significantly different from the *Mtm1* KO. Data represent mean ± S.E.M. $^{*}P < 0.05$, $^{****}P < 0.0001$ (ANOVA test).

In yeast, only MTMR2-S but not MTMR2-L regulated the PtdIns3P MTM substrate level, as well as the one of PtdIns(3,5)P_2 as assessed by vacuolar morphology (Fig. 2B). To determine whether the rescuing capacity of MTMR2 in mice was linked to its enzymatic activity, we quantified the intracellular levels of PtdIns3P in the AAV empty, MTM1, MTMR2-L and MTMR2-S injected TA muscles of *Mtm1* KO mice (Fig. 6A). PtdIns3P level was 2.3-fold higher in empty AAV injected *Mtm1* KO muscle than in WT muscle, reflecting the impact of the loss of MTM1 on its PtdIns3P lipid substrate. Upon expression of MTM1, the PtdIns3P level decreased to WT levels, reflecting the *in vivo* phosphatase activity of MTM1. Both MTMR2 isoforms induced a decrease in PtdIns3P level when expressed in the *Mtm1* KO mice, however only the short MTMR2-S isoform normalized PtdIns3P to WT levels. These results show that MTMR2 displays an *in vivo* enzymatic activity in muscle. Moreover, the MTMR2 catalytic activity correlates with the rescue observed by exogenous expression in the *Mtm1* KO myopathic mice.

Taken together, the results in *Mtm1* KO mice expressing MTM1 or MTMR2 isoforms show that the different phenotypes associated with the myopathy including reduced muscle force, myofiber atrophy, nuclei mispositioning, sarcomere and triad disorganization and increased PtdIns3P levels, were ameliorated compared with the control muscle injected with empty AAV (Table 1). Noteworthy, as observed in yeast studies, the shorter isoform MTMR2-S provided a better rescue than MTMR2-L, and was often comparable to MTM1.

Expression of the MTMR2 short isoform is reduced in the *Mtm1* KO mice muscles

Based on the GTEx expression database, the different MTMR2 mRNA variants (V1 to V4) producing these two MTMR2 protein isoforms are expressed in different tissues, with a low expression level in the skeletal muscle (Fig. 1). However, despite their strong rescue properties upon overexpression in TA muscles of *Mtm1* KO mice (Figs 3–5 and 6A; Table 1), endogenous expression of MTMR2 variants does not compensate for the loss of MTM1 function in the myopathy patients. To help understand the difference in rescue observed between the MTMR2-L and -S isoforms, we quantified mRNA levels of the different *Mtmr2* variants (V1 to V4) in TA muscles of *Mtm1* KO compared with WT mice (Fig. 6B). The results show that *Mtmr2* mRNA total level was decreased in *Mtm1* KO muscles by 2-fold. This was mainly owing to a strong decrease in the V2 and V3 transcripts encoding the MTMR2-S isoform, while the level of the V1 transcript coding for MTMR2-L remained statistically unchanged between *Mtm1* KO and WT mice. Note that these decrease were not observed in Supplementary Material, Fig. S1D since it presents a conventional RT-PCR that does not allow quantification. A similar downregulation of V2 and V3 transcripts encoding the MTMR2-S isoform was observed in XLCNM patient muscles (Fig. 6C). These data suggest that the lack of compensation of MTM1 loss by endogenous MTMR2 is linked to the low expression level of MTMR2 associated with MTMR2-S decreased level in skeletal muscles. Alternatively, this could be linked to the low level of MTMR2 proteins in the muscle.

Discussion

Here we aimed to determine functional specificities and redundancies of MTM1 and MTMR2 MTMs belonging to the same family of proteins, but whose mutations result in different diseases affecting different tissues, a myopathy and a neuropathy, respectively. We also tested their abilities to compensate for each other as a potential novel therapeutic strategy. Using molecular investigations and overexpression of these human MTMs in yeast cells and in the skeletal muscle of the *Mtm1* KO myopathic mice, we characterized two MTMR2 isoforms with different

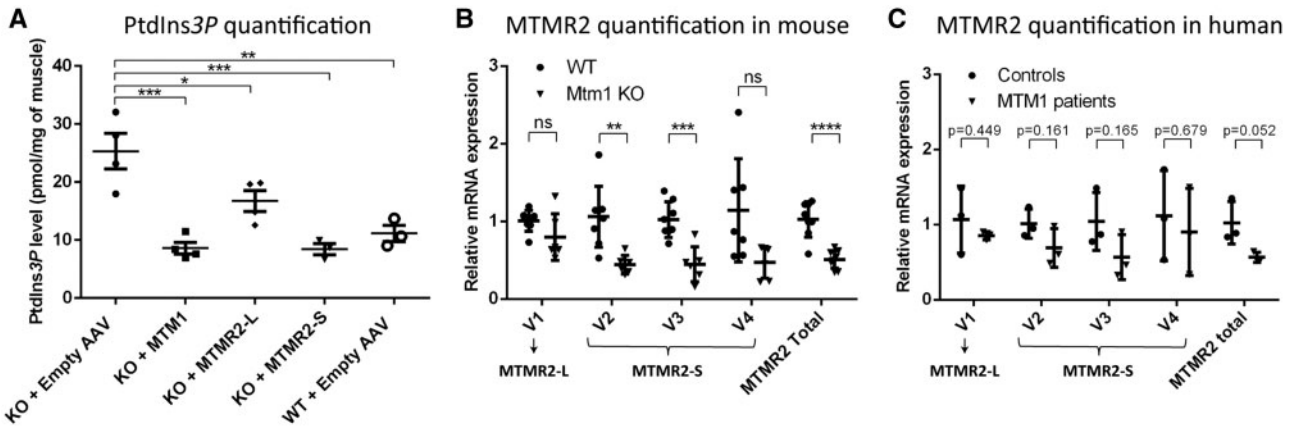

Figure 6. The MTMR2-S short isoform is reduced in the *Mtm1* KO mouse and its overexpression normalizes PtdIns3P level. **(A)** Quantification of PtdIns3P level by competitive ELISA in TA muscles from *Mtm1* KO mice expressing different myotubularins and in WT muscles. $n > 3$ mice. Data represent mean ± S.E.M. $^{*}P < 0.05$, $^{**}P < 0.01$, $^{***}P < 0.001$ (ANOVA test). PtdIns3P levels in *Mtm1* KO muscles expressing the different myotubularins are not statistically different from the WT controls. **(B)** Quantification by qRT-PCR of *Mtmr2* isoforms (V1 to V4) in the TA muscle of *Mtm1* KO mice compared with WT mice. $n > 6$. Each isoform is presented as an independent ratio, with a value of 1 set for expression in WT mice. Data represent mean ± s.d. $^{**}P < 0.01$, $^{***}P < 0.001$, $^{****}P < 0.0001$; ns, not significant (Student's *t*-test). **(C)** Quantification by qRT-PCR of *MTMR2* isoforms (V1 to V4) in muscles of patients mutated in *MTM1* compared with controls; $n = 3$. Each isoform is presented as an independent ratio, with a value of 1 set for expression in control patients. Data represent mean ± s.d. The *P* value is indicated for each isoform (Student's *t*-test).

Table 1. Rescuing effects of MTM1 and MTMR2 isoforms on several hallmarks of myotubular myopathy

	Mtm1 KO+empty AAV	*Mtm1* KO+MTM1	*Mtm1* KO+MTMR2-L	*Mtm1* KO+MTMR2-S	WT+empty AAV
Muscle weight	–	++	–	++	+++
Muscle force	–	++	+	++	+++
Fiber size	–	++	+	+	+++
Nuclei positioning	–	++	++	++	+++
Number of well-organized triads/sarcomere	–	++	+	++	+++
PtdIns3P level	–	+++	++	+++	+++

'+, ++, +++': increasing rescuing ability of myotubularins, ranging from '–': no rescue to '+++': WT phenotype.

catalytic activities linked to their ability to access their PPIn substrates. Moreover, we showed that overexpression of MTMR2 rescues the myopathy owing to MTM1 loss and that compared with MTMR2-L, the short MTMR2-S isoform displayed a better PtdIns3P phosphatase activity in yeast and in mice, correlating with better rescuing properties in MTM-depleted *ymr1*Δ yeast cells and in *Mtm1* KO mice. The fact that MTMR2-L partially improved the phenotypes of *Mtm1* KO mice despite performing poorly in yeast assays could be owing to a lack of regulatory proteins in the yeast heterologous system.

MTMR2 Isoforms and Functions

There are four naturally occurring *MTMR2* mRNA variants in human and mice encoding two protein isoforms (MTMR2-L and -S), differing by a 72 Aa extension at the N-terminal. MTMR2-S displayed a higher phosphatase activity than MTMR2-L *in vivo* in yeast and mouse, suggesting the N-terminal is important for the regulation of MTMR2 function. The phosphorylation of the serine 58, within this N-terminal extension, was shown to be important for MTMR2 endosomal membrane localization and catalytic function (33,34). Indeed, the MTMR2-S58A phosphorylation-deficient mutant was localized to membrane structures and was active towards PtdIns3P, contrary to the phosphomimetic mutant MTMR2-S58E (33,34). Here, we show that the MTMR2-S protein lacking the N-terminal sequence encompassing the S58 phosphorylated residue is concentrated to membranes when expressed in yeast (Fig. 2B) and is more active towards PtdIns3P compared with MTMR2-L in yeast (Fig. 2D) and in murine muscles (Fig. 6A). The N-terminal extension of MTMR2 was not resolved in the crystallographic structure, supporting the hypothesis that it can adopt different conformations and might regulate MTMR2 functions (24,25). These results show that there are two forms of MTMR2, MTMR2-S mainly membrane localized and with high phosphatase activity *in vivo* and MTMR2-L whose membrane localization is dependent on phosphorylation at the S58 residue. Interestingly, in brain expression is biased toward the *MTMR2* V1 variant coding for MTMR2-L (Fig. 1). The S58 phosphorylation is mediated by Erk2 kinase whose expression in brain is higher than in other tissues, correlating with MTMR2-L expression (GTEx database).

Functional Redundancy and Compensation within MTMs

There are 14 MTMs mostly ubiquitously expressed in human tissues, but the loss of MTM1 leads specifically to a severe congenital myopathy. This reveals that MTM1 homologs, notably the closer MTMR2 homolog, do not compensate for the lack of MTM1 in the skeletal muscles when expressed at endogenous levels. We provide evidence that MTMR2-S is downregulated in the skeletal muscles of the myopathic *Mtm1* KO mice and

XLCNM patients. Moreover, compared with brain and other tissues, the expression of MTMR2 transcripts is low in skeletal muscles. Altogether this suggests that this low expression of MTMR2 in muscle exacerbated by its downregulation in the myopathy mouse model and in XLCNM patient muscles is the basis for the lack of compensation. Indeed, the MTMR2-S improves better both functional and structural myopathic phenotypes and is more significantly downregulated than MTMR2-L in the myopathic muscles. This reveals that the molecular basis for the functional difference between MTM1 and MTMR2 resides in the N-terminal extension upstream the PH-GRAM domain, with the MTMR2-S lacking this extension displaying similar *in vivo* functions as MTM1 in yeast and in mice. Removal of this N-terminal extension in the native MTMR2-L isoform converts MTMR2 activity into an MTM1-like activity.

The ability of MTMR2-S to rescue myopathic phenotypes in *Mtm1* KO mice after muscle expression could be owing to the observed normalization of PtdIns3P levels. A previous study in the drosophila mutant of the *MTM1* ortholog (*mtm*) showed that impairment of class II PtdIns 3-kinase prevents the phenotypes and death of the *mtm* mutant (35). More recently, two studies proposed that normalization of PtdIns3P levels through downregulation of class II PtdIns 3-kinase PIK3C2B or broad inhibition of PtdIns 3-kinase activity and thus PtdIns3P production by Wortmannin, rescues the muscle phenotypes of *Mtm1* KO mice (36,37). Other therapeutic proof-of-concepts have been reported that do not target PPIn normalization, such as downregulation/normalization of *DNM2* (31), expression of catalytic dead MTM1-C375S (15) or inhibition of autophagy (38). Thus, it is also possible that the exogenously expressed MTMR2-L or MTMR2-S act in a PPIn-independent way to improve the *Mtm1* KO phenotypes. Of note, the MTM1-C375S dead-phosphatase mutant does not improve the triad shape that is well rescued upon expression of active MTM1 or MTMR2-S, supporting an important role of PPIn at the triad.

MTMR2 as a Novel Therapeutic Target for Myotubular Myopathy

Here we provide the proof-of-concept that MTMR2 could be used as a therapeutic target. Intramuscular AAV transduction of human MTMR2 into *Mtm1* KO mice greatly improved the phenotypes, supporting the rescue is cell autonomous in muscle. While this actual protocol aimed to investigate the cell autonomous compensation by MTMR2 through intramuscular injection, it was not possible to determine the extent of the rescue and the long-term potential of MTMR2-mediated rescue as *Mtm1* KO mice die at around 2 months most probably from respiratory failure and feeding defect. Complementation of myotubular myopathy by recombinant MTM1 or MTM1 re-expressed from injected AAVs were previously proposed as potential therapies (39,40). Expression of MTMR2 in muscle could be an attractive alternative that may not elicit immune response against the transgene, as the majority of patients with myotubular myopathy have a strong decrease or a total loss of MTM1 (41,42). Our data support that MTMR2-S isoform has a better rescuing ability than the main described MTMR2-L isoform and is a naturally occurring variant, including in muscle. Since MTMR2-S transcripts are decreased in the *Mtm1* KO muscles, a potential strategy will be to promote their expression by modulation of *MTMR2* alternative splicing or exogenous expression. Alternatively, since MTMR2 ameliorates the myopathy owing to the lack of MTM1, it would be interesting to test whether MTM1 delivery may be a therapeutic option for CMT4B caused by MTMR2 mutations.

Materials and Methods

Ethics statement

Mice were humanely killed by cervical dislocation after injection of pentobarbital, according to national and European legislations on animal experimentation.

Sample collection was performed with written informed consent from the patients or parents according to the declaration of Helsinki. The three XLCNM patients had the following mutations in *MTM1*: [c.445-49_445-4 del], [c.523A > G in exon 7, p.Arg175Gly] and [c.145_161del17 in exon 4, p.Val49Phe fs*6].

Plasmids and constructs

The human *MTM1* (1812 bp, 603 Aa) and *MTMR2-L* (1932 bp, 643 Aa) ORFs were cloned into the pDONR207 plasmid (Invitrogen, Carlsbad, CA, USA) to generate entry clones (pSF108 and pSF98, respectively). The pDONR207-MTMR2-S (1716 bp, 571 Aa, pSF101) has been obtained by site-directed mutagenesis on *MTMR2-L* into the pSF98 vector, to delete the 216 first nucleotides corresponding to the 72 first amino acids. Gateway system (Invitrogen) was used to clone the different MTM constructs into yeast destination expression vectors pAG424GPD-ccdB-EGFP (43) and pVV200 (44) obtained from the European Saccharomyces cerevisiae Archive for Functional Analysis EUROSCARF, or into a pAAV-MCS vector (CMV promoter). All constructs were verified by sequencing. The pCS211 DsRED-FYVE plasmid was previously described (27). The AAV Helper-Free system was purchased from Stratagene (La Jolla, CA) (catalog number 240071). pXR1 (AAV1) plasmid was a gift from Jude Samulski at the Gene Therapy Center, the University of North Carolina at Chapel Hill.

Antibodies

Primary antibodies used were rabbit polyclonal anti-MTM1 (2827), mouse monoclonal anti-MTMR2 (4G3), mouse monoclonal anti-phosphoglycerate Kinase 1 (PGK1, Invitrogen) and mouse monoclonal anti-glyceraldehyde-3-phosphate dehydrogenase (anti-GAPDH, Chemicon by Merk Millipore, Darmstadt, Germany). Anti-MTM1 and anti-MTMR2 antibodies were made onsite at the antibodies facility of the Institut de Génétique et Biologie Moléculaire et Cellulaire (IGBMC). Anti-MTMR2 antibodies were raised against full length human MTMR2 and validated in this study using transfected COS-7 cells. Secondary antibodies against mouse and rabbit IgG, conjugated with horseradish peroxidase (HRP) were obtained from Jackson ImmunoResearch Laboratories (West Grove, PA, USA).

In vivo models

The *S. cerevisiae ymr1Δ* (MATα, ura3-52, leu2-3,112, his3-Δ200, trp1-Δ901, lys2-801, suc2-Δ9 ymr1::HIS3) (14) and WT (MATα, his3Δ1, leu2Δ0, lys2Δ0, ura3Δ0) strains were grown at 30 °C in rich medium (YPD): 1% yeast extract, 2% peptone, 2% glucose or synthetic drop-out medium (SC): 0.67% yeast nitrogen base without amino acids, 2% glucose and the appropriate amino acids mixture to ensure plasmid maintenance. We did not use the *ymr1Δ* (MATα, his3Δ1, leu2Δ0, lys2Δ0, ura3Δ0, ymr1::KanMX) in the BY4742 background from the yeast systematic deletion

collection, because it does not have the *ymr1Δ* phenotype described by Scott D Emr's laboratory (14).

In this study, we used WT and *Mtm1* KO 129 PAS mice. The *Mtm1* KO mice are characterized by a progressive muscle atrophy and weakness starting at 2–3 weeks and leading to death by 8 weeks (30). Animals were housed in a temperature-controlled room (19–22 °C) with a 12:12-h light/dark cycle.

Bioinformatics analysis

Expression levels of *MTMR2* mRNA isoforms was obtained by mining the Genotype-Tissue Expression (GTEx, www.gtexportal.org/home/) database, which has been built by systematic RNA-sequencing using samples of 51 different tissues from hundreds of donors and two transformed cell types in culture. We then used this data to calculate the relative expression of *MTMR2* mRNA isoforms in the 20 most relevant tissues, and to create a heat map underlining in which tissue a specific isoform is the most/least expressed.

Alignment of the N-terminal part of MTM1, MTMR2-L and MTMR2-S was done using Jalview (www.jalview.org/) and aligning amino acids were identified by Clustalx color coding.

Expression analysis

Total RNA was purified from TA muscle and liver of 7-week-old WT and *Mtm1* KO mice, or from muscle biopsies of XLCNM patients and controls, using trizol reagent (Invitrogen) according to the manufacturer's instructions. cDNAs were synthesized from 500 ng of total RNA using Superscript II reverse transcriptase (Invitrogen) and random hexamers.

PCR amplification of 1/10 diluted cDNA from TA muscle and liver was performed using a forward primer from the 5'-UTR of *MTMR2*: 5'-AGCGGCCTCCAGTTTCTCGCGC-3' and a reverse primer from exon 3: 5'-TCTCTCCTGGAAGCAGGGCTGGTTCC-3', for 35 cycles of amplification at 72 °C (and 65 °C as melting temperature) and 30 min of final extension at 72 °C, as previously described (23). The products were analyzed on a 2% agarose gel, each band has been purified using Nucleospin Gel and PCR cleanup kit (Macherey-Nagel, Düren, Germany), then cloned into a pJet2.1 vector using the CloneJet PCR cloning kit (ThermoFisher Scientific, Waltham, MA, USA), and sequenced by Sanger.

Quantitative PCR amplification of 1/10 diluted cDNAs from mouse TA muscles or human muscle biopsies was performed on Light-Cycler 480 II instrument (Roche, Basel, Swiss) using 53 °C as melting temperature. Specific sets of primers were used for each mouse *MTMR2* isoform: forward 5'-GACTCACTGTCC AGTGCTTC-3' and reverse 5'-CCTCCCTCAGGACCCTCA-3' for mouse V1, forward 5'-GACTCACTGTCCAGTGCTTC-3' and reverse 5'-CAGCTGGGCACTCCCTCA-3' for mouse V2, forward 5'-AAGATAAAACATCTCAAAAATTATAATTGCTTC-3' and reverse 5'-CAGCTGGGCACTCCCTCA-3' for mouse V3, forward 5'-AAGATAAAACATCTCAAAAATTATAATTGCTTC-3' and reverse 5'-GACTCACTGTCCAGTGCTTC-3' for mouse V4. Another set of primers (forward 5'-TCCTGTGTCTAATGGCTTGC-3' and reverse 5'-AACCAAGAGGGCAGGATATG-3') amplifying a sequence common to all mouse isoforms has been used to quantify total mouse MTMR2. Other specific sets of primers were used for each human *MTMR2* isoform: forward 5'-ACTCCTTGTCCAG TGCCTC-3' and reverse 5'-GACTCCCTCAGGACCCTC-3' for human V1, forward 5'-AAGATAAAACATCTCAAAAATTATAATT GCCTC-3' and reverse 5'-GACTCCCTCAGGACCCTC-3' for human V2, forward 5'-AAGATAAAACATCTCAAAAATTATAATTGCCTC-3' and reverse 5'-GAGCGAGACTCCCTCCTC-3' for human V3, forward 5'-AAGATAAAACATCTCAAAAATTATAATTGCCTC-3' and reverse 5'-CTGGACTGCATGGGCCTC-3' for human V4. Another set of primers (forward 5'-TTTCCTGTCTCTAATAACCTGCC-3' and reverse 5'-CCAGGAGGGCAGGGTATG-3') amplifying a sequence common to all human isoforms has been used to quantify total human MTMR2. For all qPCR, the *HPRT* gene expression was used as control because of the non-variation in its expression between control and XLCNM muscles.

Western blot

Total proteins were extracted from yeast cells (OD_{600nm} = 0.5–0.9, minimum three clones per construct) by TCA precipitation and NaOH lysis (45), and from TA muscles (minimum 10 muscles per construct) by homogenization in RIPA buffer using a tissue homogenizer (Omni TH, Kennesaw, GA, USA). Protein lysates were analyzed by SDS-PAGE and western blotting on nitrocellulose membrane. Proteins were detected using primary antibody (anti-MTM1 1/500, anti-MTMR2 1/1000, anti-PGK1 1/1000 and anti-GAPDH 1/1000) followed by incubation with the secondary antibody coupled to HRP, and extensive washing. Membranes were revealed by ECL chemiluminescent reaction kit (Supersignal west pico kit, ThermoFisher Scientific).

Yeast phenotyping

ymr1Δ yeast cells were transformed using the LiAc-PEG method (46) by yeast expression plasmids pAG424GPD-ccdB-EGFP (2μ, GFP tag at C-ter) or pVV200 (2μ, no tag) containing *MTM1*, *MTMR2-L* or *MTMR2-S* cDNA. Yeast cells transformed by empty plasmids were used as controls.

For vacuole staining, 1 OD_{600nm} unit of cells was harvested by a 500*g* centrifugation for 1 min, incubated in 50 μl YPD medium with 2 μl FM4-64 (200 μM, Invitrogen) for 15 min at 30 °C, prior washing with 900 μl YPD and chasing by incubation at 30 °C for 10 min followed by a second wash in SC complete medium, the stained living yeast cells were observed by fluorescent microscopy. Between 100 and 600 cells per clone (three different clones per construct) were counted and classified into 2 categories: large or medium unilobar vacuole, and small or fragmented vacuole.

For PtdIns3P quantification, yeast cells were co-transformed by a pVV200 plasmid (empty or containing *MTM1*, *MTMR2-L* or *MTMR2-S* cDNA) and the pCS211 plasmid expressing the DsRED-FYVE reporter for PtdIns3P-enriched membrane structures (27). After fluorescence microscopy, the number of dots per cell was quantified on minimum 100 cells per clone (2 different clones per construct).

For PtdIns5P quantification, yeast *ymr1Δ* cells producing the different MTM1 and MTMR2 constructs were grown to exponential phase. Lipid extraction was done as described in Hama *et al.* on 200 OD_{600nm} units of cells (47). Quantification of the PtdIns(5)P level was performed as described by Morris *et al.* (48) and the results were normalized based on the total lipid concentration.

All fluorescence microscopy observations were done with 100×/1.45 oil objective (Zeiss) on a fluorescence Axio Observer D1 microscope (Zeiss) using GPF or DsRED filter and DIC optics. Images were captured with a CoolSnap HQ2 photometrix camera (Roper Scientific) and treated by ImageJ (Rasband W.S., ImageJ, U. S. National Institutes of Health, Bethesda, MD, USA, http://imagej.nih.gov/ij/; date last accessed July 11, 2017).

PtdIns3P quantification by ELISA in muscle extracts

PtdIns3P Mass ELISAs were performed on lipid extracts from whole TA muscle preparations according to the manufacturer's recommendations and using the PtdIns3P Mass ELISA kit (Echelon Biosciences, Salt Lake City, UT, USA). TA muscles from 7-week-old WT of *Mtm1* KO mice were weighed, grinded into a powder using a mortar and pestle under liquid nitrogen and then incubated in ice cold 5% TCA to extract lipids. Extracted lipids were resuspended in PBS-T with 3% protein stabilizer and then spotted on PtdIns3P Mass ELISA plates in duplicates. PtdIns3P levels were detected by measuring absorbance at 450 nm on a plate reader. Specific amounts were determined by comparison of values to a standard curve generated with known amounts of PtdIns3P.

AAV production

rAAV2/1 vectors were generated by a triple transfection of AAV-293 cell line with pAAV2-insert containing the insert under the control of the CMV promoter and flanked by serotype-2 inverted terminal repeats, pXR1 containing *rep* and *cap* genes of AAV serotype-1, and pHelper encoding the adenovirus helper functions. Viral vectors were purified and quantified by real time PCR using a plasmid standard pAAV-eGFP. Titers are expressed as viral genomes per ml (vg/ml) and rAAV titers used here were $5–7\times10^{11}$ vg/ml.

AAV transduction of TA muscles of WT and *Mtm1* KO mice

Two- to 3-week-old WT or *Mtm1* KO male 129PAS mice were anesthetized by intraperitoneal injection of 5 ml/g of ketamine (20 mg/ml; Virbac, Carros, France) and xylazine (0.4%, Rompun; Bayer, Wuppertal, Germany). TA muscles were injected with 20 µl of AAV2/1 preparations or sterile AAV2/1 empty vector. Four weeks later, mice were anesthetized and the TA muscle was either functionally analyzed (as described below), or directly dissected and frozen in nitrogen-cooled isopentane for histology, or fixed for electron microscopy (as described below).

Functional analysis of the muscle

Muscle force measurements were evaluated by measuring *in situ* muscle contraction in response to nerve and muscle stimulation, as described previously (31). Animals were anesthetized by intraperitoneal injection of pentobarbital sodium (50 mg/kg). The distal tendon of the TA was detached and tied with a silk ligature to an isometric transducer (Harvard Bioscience, Holliston, MA, USA). The sciatic nerve was distally stimulated, response to tetanic stimulation (pulse frequency of 50–143 Hz) was recorded, and absolute maximal force was determined. After contractile measurements, the animals were sacrificed by cervical dislocation. To determine specific maximal force, TA muscles were dissected and weighed.

Histology

Transverse cryosections (9 µm) of mouse TA skeletal muscles were stained with hematoxylin and eosin (HE) or SDH and viewed with a NanoZoomer 2.0HT slide scanner (Hamamatsu, Hamamatsu city, Japan). Fiber area was analyzed on HE sections, using the RoiManager plugin of ImageJ image analysis software. The percentage of peripheral nuclei was counted using the cell counter plugin of ImageJ image analysis software.

Electron microscopy

TA muscles of anesthetized mice were fixed with 4% PFA and 2.5% glutaraldehyde in 0.1 M phosphate buffer (pH 7.2) and processed as described (49). Ratio of triads/sarcomere was calculated by dividing the number of triad structures identified by the total number of sarcomeres present on the section (2 mice per genotype, minimum 10 fibers analyzed per mice, minimum 20 triads per fiber).

Statistical analysis

Data are mean ± S.E.M. or ±SD as noted in the figure legend. Statistical analysis was performed using one-way ANOVA followed by Tukey's multiple comparisons test for all data except for the expression analysis (Fig. 6B and C) where an unpaired two-tailed Student's *t* test was performed. A P value <0.05 was considered significant.

Supplementary Material

Supplementary Material is available at *HMG* online.

Authors' Contribution

J.L., S.F. and B.C. provided direction for the project, conceived and designed the experiments; D.L.B. and M.R. performed yeast experiments and data analyses; J.M.X. and B.P. performed the PI5P mass assay on total lipid extracts from yeast; B.R. and D.L.B. constructed the yeast expression plasmids; M.R. constructed the AAV plasmids; M.R. and B.C. designed and performed the mice experiments and data analyses; M.R. performed the experiment on human biopsies; N.R. provided the human muscle biopsies; C.K. maintained the mouse lines and did the genotyping; P.K. conceived an ImageJ macro to analyze the nuclei positioning; M.R., J.L., S.F and B.C. analyzed the data and wrote the manuscript.

Acknowledgements

We thank Raphael Schneider, Hichem Tasfaout, Pascale Koebel, Nadia Messadeq, Josiane Hergueux, Coralie Spiegelhalter for excellent technical assistance. We thank Scott D. Emr (Cornell University, USA) and Christopher J. Stefan (University College London, UK) for sharing yeast strains and plasmids. We thank V. Laugel (Strasbourg hospital, France) for sharing an XLCNM patient muscle biopsy. We thank the very helpful platforms of the IGBMC: the imaging center, the antibodies facility, the animal house, the cell culture facility, and the molecular biology facility.

Conflict of Interest statement. None declared.

Funding

This work was supported by the Centre National de la Recherche Scientifique (CNRS); the Institut National de la Santé et de la Recherche Médicale (INSERM); Université de Strasbourg; the Agence Nationale de la Recherche [ANR-13-BSV2-0004 to S.F. and J.L., ANR-10-LABX-0030-INRT, ANR-10-IDEX-0002-02]; E-

rare [11-040 to J.L.]; and the Association Française contre les Myopathies AFM-Téléthon [AFM 2013-0133/16551 to S.F. and PhD fellowship to M.R.].

References

1. Raess, M.A., Friant, S., Cowling, B.S. and Laporte, J. (2017) WANTED - Dead or alive: Myotubularins, a large disease-associated protein family. *Advances in biological regulation*, **63**, 49–58.
2. Blondeau, F., Laporte, J., Bodin, S., Superti-Furga, G., Payrastre, B. and Mandel, J.L. (2000) Myotubularin, a phosphatase deficient in myotubular myopathy, acts on phosphatidylinositol 3-kinase and phosphatidylinositol 3-phosphate pathway. *Hum. Mol. Genet.*, **9**, 2223–2229.
3. Taylor, G.S., Maehama, T. and Dixon, J.E. (2000) Inaugural article: myotubularin, a protein tyrosine phosphatase mutated in myotubular myopathy, dephosphorylates the lipid second messenger, phosphatidylinositol 3-phosphate. *Proc. Natl. Acad. Sci. U. S. A.*, **97**, 8910–8915.
4. Vicinanza, M., D'Angelo, G., Di Campli, A. and De Matteis, M.A. (2008) Function and dysfunction of the PI system in membrane trafficking. *EMBO J.*, **27**, 2457–2470.
5. Tronchere, H., Laporte, J., Pendaries, C., Chaussade, C., Liaubet, L., Pirola, L., Mandel, J.L. and Payrastre, B. (2004) Production of phosphatidylinositol 5-phosphate by the phosphoinositide 3-phosphatase myotubularin in mammalian cells. *J. Biol. Chem.*, **279**, 7304–7312.
6. Walker, D.M., Urbe, S., Dove, S.K., Tenza, D., Raposo, G. and Clague, M.J. (2001) Characterization of MTMR3. an inositol lipid 3-phosphatase with novel substrate specificity. *Curr. Biol.*, **11**, 1600–1605.
7. Berger, P., Bonneick, S., Willi, S., Wymann, M. and Suter, U. (2002) Loss of phosphatase activity in myotubularin-related protein 2 is associated with Charcot-Marie-Tooth disease type 4B1. *Hum. Mol. Genet.*, **11**, 1569–1579.
8. Jin, N., Lang, M.J. and Weisman, L.S. (2016) Phosphatidylinositol 3,5-bisphosphate: regulation of cellular events in space and time. *Biochem. Soc. Trans.*, **44**, 177–184.
9. Schink, K.O., Raiborg, C. and Stenmark, H. (2013) Phosphatidylinositol 3-phosphate, a lipid that regulates membrane dynamics, protein sorting and cell signalling. *BioEssays*, **35**, 900–912.
10. Berger, P., Berger, I., Schaffitzel, C., Tersar, K., Volkmer, B. and Suter, U. (2006) Multi-level regulation of myotubularin-related protein-2 phosphatase activity by myotubularin-related protein-13/set-binding factor-2. *Hum. Mol. Genet.*, **15**, 569–579.
11. Kim, S.A., Vacratsis, P.O., Firestein, R., Cleary, M.L. and Dixon, J.E. (2003) Regulation of myotubularin-related (MTMR)2 phosphatidylinositol phosphatase by MTMR5, a catalytically inactive phosphatase. *Proc. Natl. Acad. Sci. U. S. A.*, **100**, 4492–4497.
12. Nandurkar, H.H., Layton, M., Laporte, J., Selan, C., Corcoran, L., Caldwell, K.K., Mochizuki, Y., Majerus, P.W. and Mitchell, C.A. (2003) Identification of myotubularin as the lipid phosphatase catalytic subunit associated with the 3-phosphatase adapter protein, 3-PAP. *Proc. Natl. Acad. Sci. U. S. A.*, **100**, 8660–8665.
13. Lecompte, O., Poch, O. and Laporte, J. (2008) PtdIns5P regulation through evolution: roles in membrane trafficking? *Trends Biochem. Sci.*, **33**, 453–460.
14. Parrish, W.R., Stefan, C.J. and Emr, S.D. (2004) Essential role for the myotubularin-related phosphatase Ymr1p and the synaptojanin-like phosphatases Sjl2p and Sjl3p in regulation of phosphatidylinositol 3-phosphate in yeast. *Mol. Biol. Cell*, **15**, 3567–3579.
15. Amoasii, L., Bertazzi, D.L., Tronchere, H., Hnia, K., Chicanne, G., Rinaldi, B., Cowling, B.S., Ferry, A., Klaholz, B., Payrastre, B. *et al.* (2012) Phosphatase-dead myotubularin ameliorates X-linked centronuclear myopathy phenotypes in mice. *PLoS Genet.*, **8**, e1002965.
16. Laporte, J., Hu, L.J., Kretz, C., Mandel, J.L., Kioschis, P., Coy, J.F., Klauck, S.M., Poustka, A. and Dahl, N. (1996) A gene mutated in X-linked myotubular myopathy defines a new putative tyrosine phosphatase family conserved in yeast. *Nat. Genet.*, **13**, 175–182.
17. Bolino, A., Muglia, M., Conforti, F.L., LeGuern, E., Salih, M.A., Georgiou, D.M., Christodoulou, K., Hausmanowa-Petrusewicz, I., Mandich, P., Schenone, A. *et al.* (2000) Charcot-Marie-Tooth type 4B is caused by mutations in the gene encoding myotubularin-related protein-2. *Nat. Genet.*, **25**, 17–19.
18. Senderek, J., Bergmann, C., Weber, S., Ketelsen, U.P., Schorle, H., Rudnik-Schoneborn, S., Buttner, R., Buchheim, E. and Zerres, K. (2003) Mutation of the SBF2 gene, encoding a novel member of the myotubularin family, in Charcot-Marie-Tooth neuropathy type 4B2/11p15. *Hum. Mol. Genet.*, **12**, 349–356.
19. Azzedine, H., Bolino, A., Taieb, T., Birouk, N., Di Duca, M., Bouhouche, A., Benamou, S., Mrabet, A., Hammadouche, T., Chkili, T. *et al.* (2003) Mutations in MTMR13, a new pseudophosphatase homologue of MTMR2 and Sbf1, in two families with an autosomal recessive demyelinating form of Charcot-Marie-Tooth disease associated with early-onset glaucoma. *Am. J. Hum. Genet.*, **72**, 1141–1153.
20. Alazami, A.M., Alzahrani, F., Bohlega, S. and Alkuraya, F.S. (2014) SET binding factor 1 (SBF1) mutation causes Charcot-Marie-tooth disease type 4B3. *Neurology*, **82**, 1665–1666.
21. Manole, A., Horga, A., Gamez, J., Raguer, N., Salvado, M., San Millan, B., Navarro, C., Pittmann, A., Reilly, M.M. and Houlden, H. (2017) SBF1 mutations associated with autosomal recessive axonal neuropathy with cranial nerve involvement. *Neurogenetics*, **18**, 63–67.
22. Nakhro, K., Park, J.M., Hong, Y.B., Park, J.H., Nam, S.H., Yoon, B.R., Yoo, J.H., Koo, H., Jung, S.C., Kim, H.L. *et al.* (2013) SET binding factor 1 (SBF1) mutation causes Charcot-Marie-Tooth disease type 4B3. *Neurology*, **81**, 165–173.
23. Bolino, A., Marigo, V., Ferrera, F., Loader, J., Romio, L., Leoni, A., Di Duca, M., Cinti, R., Cecchi, C., Feltri, M.L. *et al.* (2002) Molecular characterization and expression analysis of Mtmr2, mouse homologue of MTMR2, the Myotubularin-related 2 gene, mutated in CMT4B. *Gene*, **283**, 17–26.
24. Begley, M.J., Taylor, G.S., Brock, M.A., Ghosh, P., Woods, V.L. and Dixon, J.E. (2006) Molecular basis for substrate recognition by MTMR2, a myotubularin family phosphoinositide phosphatase. *Proc. Natl. Acad. Sci. U. S. A.*, **103**, 927–932.
25. Begley, M.J., Taylor, G.S., Kim, S.A., Veine, D.M., Dixon, J.E. and Stuckey, J.A. (2003) Crystal structure of a phosphoinositide phosphatase, MTMR2: insights into myotubular myopathy and Charcot-Marie-Tooth syndrome. *Mol. Cell*, **12**, 1391–1402.
26. GTEx_consortium. (2015) Human genomics. The genotype-tissue expression (GTEx) pilot analysis: multitissue gene regulation in humans. *Science*, **348**, 648–660.
27. Katzmann, D.J., Stefan, C.J., Babst, M. and Emr, S.D. (2003) Vps27 recruits ESCRT machinery to endosomes during MVB sorting. *J. Cell Biol.*, **162**, 413–423.

28. Cooke, F.T., Dove, S.K., McEwen, R.K., Painter, G., Holmes, A.B., Hall, M.N., Michell, R.H. and Parker, P.J. (1998) The stress-activated phosphatidylinositol 3-phosphate 5-kinase Fab1p is essential for vacuole function in *S. cerevisiae*. *Curr. Biol.*, **8**, 1219–1222.
29. Dove, S.K., Cooke, F.T., Douglas, M.R., Sayers, L.G., Parker, P.J. and Michell, R.H. (1997) Osmotic stress activates phosphatidylinositol-3,5-bisphosphate synthesis. *Nature*, **390**, 187–192.
30. Buj-Bello, A., Laugel, V., Messaddeq, N., Zahreddine, H., Laporte, J., Pellissier, J.F. and Mandel, J.L. (2002) The lipid phosphatase myotubularin is essential for skeletal muscle maintenance but not for myogenesis in mice. *Proc. Natl. Acad. Sci. U. S. A.*, **99**, 15060–15065.
31. Cowling, B.S., Chevremont, T., Prokic, I., Kretz, C., Ferry, A., Coirault, C., Koutsopoulos, O., Laugel, V., Romero, N.B. and Laporte, J. (2014) Reducing dynamin 2 expression rescues X-linked centronuclear myopathy. *J. Clin. Invest.*, **124**, 1350–1363.
32. Spiro, A.J., Shy, G.M. and Gonatas, N.K. (1966) Myotubular myopathy. Persistence of fetal muscle in an adolescent boy. *Arch. Neurol.*, **14**, 1–14.
33. Franklin, N.E., Bonham, C.A., Xhabija, B. and Vacratsis, P.O. (2013) Differential phosphorylation of the phosphoinositide 3-phosphatase MTMR2 regulates its association with early endosomal subtypes. *J. Cell Sci.*, **126**, 1333–1344.
34. Franklin, N.E., Taylor, G.S. and Vacratsis, P.O. (2011) Endosomal targeting of the phosphoinositide 3-phosphatase MTMR2 is regulated by an N-terminal phosphorylation site. *J. Biol. Chem.*, **286**, 15841–15853.
35. Velichkova, M., Juan, J., Kadandale, P., Jean, S., Ribeiro, I., Raman, V., Stefan, C. and Kiger, A.A. (2010) Drosophila Mtm and class II PI3K coregulate a PI(3)P pool with cortical and endolysosomal functions. *J. Cell Biol*, **190**, 407–425.
36. Kutchukian, C., Lo Scrudato, M., Tourneur, Y., Poulard, K., Vignaud, A., Berthier, C., Allard, B., Lawlor, M.W., Buj-Bello, A. and Jacquemond, V. (2016) Phosphatidylinositol 3-kinase inhibition restores Ca2+ release defects and prolongs survival in myotubularin-deficient mice. *Proc. Natl. Acad. Sci. U. S. A.*, **113**, 14432–14437.
37. Sabha, N., Volpatti, J.R., Gonorazky, H., Reifler, A., Davidson, A.E., Li, X., Eltayeb, N.M., Dall'Armi, C., Di Paolo, G., Brooks, S.V. *et al.* (2016) PIK3C2B inhibition improves function and prolongs survival in myotubular myopathy animal models. *J. Clin. Invest.*, **126**, 3613–3625.
38. Fetalvero, K.M., Yu, Y., Goetschkes, M., Liang, G., Valdez, R.A., Gould, T., Triantafellow, E., Bergling, S., Loureiro, J., Eash, J. *et al.* (2013) Defective autophagy and mTORC1 signaling in myotubularin null mice. *Mol. Cell. Biol*, **33**, 98–110.
39. Childers, M.K., Joubert, R., Poulard, K., Moal, C., Grange, R.W., Doering, J.A., Lawlor, M.W., Rider, B.E., Jamet, T., Daniele, N. *et al.* (2014) Gene therapy prolongs survival and restores function in murine and canine models of myotubular myopathy. *Sci Transl Med*, **6**, 220ra210.
40. Lawlor, M.W., Armstrong, D., Viola, M.G., Widrick, J.J., Meng, H., Grange, R.W., Childers, M.K., Hsu, C.P., O'Callaghan, M., Pierson, C.R. *et al.* (2013) Enzyme replacement therapy rescues weakness and improves muscle pathology in mice with X-linked myotubular myopathy. *Hum. Mol. Genet.*, **22**, 1525–1538.
41. Laporte, J., Biancalana, V., Tanner, S.M., Kress, W., Schneider, V., Wallgren-Pettersson, C., Herger, F., Buj-Bello, A., Blondeau, F., Liechti-Gallati, S. *et al.* (2000) MTM1 mutations in X-linked myotubular myopathy. *Hum. Mutat.*, **15**, 393–409.
42. Laporte, J., Kress, W. and Mandel, J.L. (2001) Diagnosis of X-linked myotubular myopathy by detection of myotubularin. *Ann. Neurol.*, **50**, 42–46.
43. Alberti, S., Gitler, A.D. and Lindquist, S. (2007) A suite of Gateway cloning vectors for high-throughput genetic analysis in *Saccharomyces cerevisiae*. *Yeast*, **24**, 913–919.
44. Van Mullem, V., Wery, M., De Bolle, X. and Vandenhaute, J. (2003) Construction of a set of Saccharomyces cerevisiae vectors designed for recombinational cloning. *Yeast*, **20**, 739–746.
45. Volland, C., Urban-Grimal, D., Geraud, G. and Haguenauer-Tsapis, R. (1994) Endocytosis and degradation of the yeast uracil permease under adverse conditions. *J. Biol. Chem.*, **269**, 9833–9841.
46. Gietz, D., St Jean, A., Woods, R.A. and Schiestl, R.H. (1992) Improved method for high efficiency transformation of intact yeast cells. *Nucleic Acids Res.*, **20**, 1425.
47. Hama, H., Takemoto, J.Y. and DeWald, D.B. (2000) Analysis of phosphoinositides in protein trafficking. *Methods*, **20**, 465–473.
48. Morris, J.B., Hinchliffe, K.A., Ciruela, A., Letcher, A.J. and Irvine, R.F. (2000) Thrombin stimulation of platelets causes an increase in phosphatidylinositol 5-phosphate revealed by mass assay. *FEBS Lett.*, **475**, 57–60.
49. Cowling, B.S., Toussaint, A., Amoasii, L., Koebel, P., Ferry, A., Davignon, L., Nishino, I., Mandel, J.L. and Laporte, J. (2011) Increased expression of wild-type or a centronuclear myopathy mutant of dynamin 2 in skeletal muscle of adult mice leads to structural defects and muscle weakness. *Am. J. Pathol.*, **178**, 2224–2235.